

A Zero-Equation Model for External Aerodynamics

M. M. Rahman^{1*}, Xueting Zhang², K. Hasan³, and Sheng Chen⁴

Hangzhou Dianzi University, School of Mechanical Engineering, 310018 Hangzhou, China

emails: ¹mizanur_rahman@hdu.edu.cn; ²zxt@hdu.edu.cn; ³m.k.hasan@hdu.edu.cn; and ⁴chensh@hdu.edu.cn

ARTICLE INFO

Article History:

Received: 17th January 2023

Revised: 17th April 2023

Accepted: 26th April 2023

Published: 25th June 2023

Keywords:

Zero-equation model

Dilation symmetry

Stress length

order function

Wall turbulence

ABSTRACT

The zero-equation model (ZEM) has been generalized for aerodynamic applications by eliminating the thickness of boundary-layer (BL) dependency to construct the stress length parameter l_{12} . The SED (Structural Ensemble Dynamics) postulate evaluates the l_{12} using the order function based on universal multi-layer structures for wall turbulence. The SED concept is further employed to optimize the profiles of the turbulent kinetic energy and dissipation rate with turbulent BL flows. Results demonstrate that the multi-layer ZEM receives a remarkable achievement in the prediction of wall-bounded turbulence and thus, prevails over the drawbacks encountered in most algebraic turbulence models.

© 2023 MIJST. All rights reserved.

NOMENCLATURE

AOA	angle of attack	u_τ	wall-friction velocity
BL	boundary layer	Y	distance to wall
C	airfoil cord length	y^+	wall distance parameter; $u_\tau y/v$
DI	dilation invariance	ZEM	zero-equation model
DS	dilation symmetry	δ	BL thickness
K	kinetic energy of turbulence	ϵ	rate of turbulence dissipation
l_{12}	stress length	κ	von-Karman constant
P	pressure	μ, μ_T	laminar & eddy viscosities
R_b	factor of stress-intensity	ν	laminar kinematic viscosity
Re	Reynolds number	ρ	density
R_T	eddy-to-laminar viscosity ratio		
S	mean strain-rate tensor		
SED	structural ensemble dynamics		
SST	shear stress transport		
u_i	velocity vector		

1. INTRODUCTION

To develop a zero-equation model (ZEM), the correlation-based turbulence modelling with a dimensional argument may induce lots of functions and coefficients which lack physical interpretations (Wilcox, 2006). The devised turbulence model with this inconsistent aspect typically inherits unexpected complications to accurately predict the flow with practical features. However, the physical understanding of the universal structure related to wall turbulence can provide a compelling route to format a ZEM in conjunction with “Reynolds-averaged Navier-

Stokes (RANS)” equations. The current research applies a well-established physics of wall turbulence to formulate a plausible ZEM, which is unfortunately beyond the capacity of the mixing length hypothesis of Prandtl (1925), von Karman lag-law theory (Segalini, 2013) and Townsend similarity argument (1976).

The “SED theory” of She *et al.* (2010, 2017, and 2009) aims at using the turbulence statistical symmetry to make a quantitative description of the wall-bounded turbulence feasible. The dilation symmetry (DS) deserves an outstanding significance due to a universal wall constraint

on turbulence eddies, since the DS determines the solutions to RANS equations through the relevant order parameter/function (whose role of symmetry remains prevalent to wall flows), describing ensemble properties emerged from turbulence fluctuations which restore a DS (layer by layer) and the order-function scaling can quantify the symmetry property (She *et al.*, 2017). More precisely, the mean velocity is altered by inherent turbulence fluctuations in association with the Reynolds stress leading to symmetry breaking; however, a length order function can handle this interaction (effect) with its dilation-invariance (DI) scaling, showing a perceptible nature from one layer to another. Under a “generalized Lie-group” DI, the SED concept employs a multi-layer formulation of the order function (key to quantifying turbulence) to speculate the stress length l_{12} with a fully-developed turbulent BL flow. The analytic profile is ended up with “four-layer structures”, consisting of a viscous sublayer, buffer layer, bulk flow region (retaining log-layer) and core layer. Apparently, variances among different layers of a physical flow domain can be represented by the variations (layer-to-layer transition sharpness and scaling) in multi-layer parameters.

A ZEM has been recently developed using the SED concept (wall-turbulence with distinct multi-layer physics) (Rahman *et al.* 2021), where the kinematic eddy-viscosity is evaluated as $\nu_T = l_{12}^2 S$ with the strain-rate invariant S . The “Bradshaw stress-intensity parameter” R_b (Bradshaw, 1967) which is a function of an eddy-to-laminar viscosity ratio R_T has been used to model the turbulent kinetic energy k and dissipation-rate \mathcal{E} . The resulting ZEM provides reasonable predictions for a fully-developed channel flow. However, the ZEM needs to evaluate boundary layer (BL) thickness parameter δ in forming the stress length l_{12} , which is difficult to be included in three-dimensional numerical algorithms. More specifically, aerodynamic applications usually integrate the BL influence of the wall curvature, although the BL edge is not well-defined, reflecting numerical confusion to accurately determine δ . This deficiency has been eliminated from the stress length l_{12} by replacing the bulk flow region and core layer with an additional transition layer (log-layer) and the celebrated matching layer.

Improved $k-\mathcal{E}$ analytic profiles are obtained as a combination of the Bradshaw parameter and another optimized k profile for a fully-developed BL flow using the SED hypothesis. A cursory examination approves that the multi-layer ZEM dominates over the past developed algebraic turbulence models (Prandtl, 1925; Segalini *et al.*, 2013; Townsend, 1976; and Wilcox, 2006).

2. GOVERNING EQUATIONS

In collaboration with the RANS turbulence modelling, the turbulent eddy-viscosity μ_T has been evaluated by the stress length scale with regards to the “SED theory”. The

RANS equations describe the physics of a continuum medium using the mean conservations of mass, momentum and energy. The differential formulations in tensor form read:

$$\frac{\partial \rho}{\partial t} + \frac{\partial(\rho u_i)}{\partial x_i} = 0 \tag{1}$$

$$\frac{\partial \rho u_i}{\partial t} + \frac{\partial}{\partial x_j} (\rho u_i u_j) = -\frac{\partial p}{\partial x_i} + \frac{\partial \sigma_{ij}}{\partial x_j} \tag{2}$$

$$\begin{aligned} \frac{\partial}{\partial t} \left(\rho e + \frac{\rho u_i^2}{2} \right) + \frac{\partial}{\partial x_j} \left[\rho u_j \left(h + \frac{u_i^2}{2} \right) \right] \\ = \frac{\partial u_i \sigma_{ij}}{\partial x_j} - \frac{\partial}{\partial x_j} \left[\left(\frac{\mu}{Pr} + \frac{\mu_T}{Pr_T} \right) \frac{\partial T}{\partial x_j} \right] \end{aligned} \tag{3}$$

where ρ the fluid density, p the static pressure, u_i the i th component of velocity and x_i the Cartesian coordinates, e the specific internal energy, and $h = e + p/\rho$ represents the specific enthalpy. The working fluid is air; the laminar Prandtl number $Pr = 0.7$ and turbulent Prandtl number Pr_T is set to 0.9. The laminar viscosity μ is calculated from Sutherland’s formula. The “equation of state” is $p = \rho RT$ for a calorically perfect fluid, where R the perfect gas constant and T the absolute temperature. Additionally, $e = C_v T$ and $h = C_p T$, where C_v and C_p are the specific heat coefficients at constant volume and pressure, respectively.

The “Boussinesq approximation” can be used to relate the total stresses σ_{ij} with the “mean strain-rate tensor” S_{ij} as:

$$\begin{aligned} \sigma_{ij} &= 2(\mu + \mu_T) \left(S_{ij} - \frac{1}{3} S_{kk} \delta_{ij} \right), \\ S_{ij} &= \frac{1}{2} \left(\frac{\partial u_i}{\partial x_j} + \frac{\partial u_j}{\partial x_i} \right) \end{aligned} \tag{4}$$

where δ_{ij} implies Kronecker’s delta function with $\delta_{ij} = 1$ for $i = j$ and $\delta_{ij} = 0$ for $i \neq j$. The “SED theory” applies the stress length function l_{12} to define μ_T as:

$$\mu_T = \rho \nu_T = \rho l_{12}^2 S \tag{5}$$

where $S = \sqrt{2 S_{ij} S_{ij}}$ is the mean strain-rate invariant.

The “SED theory” states that a proper set of order functions can represent the wall turbulence, retaining complex systems with multi-layer structures (She *et al.* 2010). A quantitative analysis of the “generalized Lie-group” DI can be applied to deduce the characteristic order function (in a framework of

multi-products) as the wall is present. The generic form of the order function ϕ with complex multi-layer structures can be given as (She et al., 2017):

$$\phi = c_0 \left(\frac{y}{a_0} \right)^{c_0/b_0} \prod_{i=1}^n \left[1 + \left(\frac{y}{a_i} \right)^{b_i} \right]^{c_i/b_i} \quad (6)$$

where ϕ is parameterized with a variable y ; adjustable constants are $(a, b \ \& \ c)$ with the number of products, n . In principle, multiple transitions from one layer to another occur due to the spatial variation of ϕ . Naturally, the stress length l_{12} associates multi-layer features in a fully-developed turbulent BL, as supported by the SED hypothesis, which provides the formulation of l_{12} for a fully-developed channel flow as (She et al., 2017):

$$l_{12}^+ = l_0 \left(\frac{y^+}{9.7} \right)^{3/2} \left[1 + \left(\frac{y^+}{9.7} \right)^4 \right]^{1/8} \left[1 + \left(\frac{y^+}{41} \right)^4 \right]^{-1/4} \frac{1-r^4}{4(1-r)} \left[1 + \left(\frac{0.27}{r} \right)^2 \right]^{1/4} \quad (7)$$

where the non-dimensional wall-distance $y^+ = yu_\tau/\nu$ with the “wall-friction velocity” $u_\tau = \sqrt{(\nu S)_w}$ and laminar kinematic viscosity $\nu = \mu/\rho$. Note that u_τ can be regarded as a well-defined parameter as long as $S_w > 0$. Additionally, $r = 1 - y/\delta = 1 - y^+/\text{Re}_\tau$ implies the distance from the channel center-line, where the channel half-width δ and friction Reynolds number $\text{Re}_\tau = \delta u_\tau/\nu$. Equation (7) describes canonical four-layer structures (as mentioned earlier) of wall turbulence with a fully-developed BL channel flow. The extension of each layer is identified empirically by its layer thickness. They are the viscous sublayer at $y_{sub}^+ = 9.7$, buffer layer at $y_{buf}^+ = 41$, core layer with a core layer thickness of $r_{core} = 0.27$ and bulk-flow region. A detailed description of the various layers can be found in Reference (Rahman et al., 2021). Note that the geometry-dependent bulk-flow structure $1 - r^4$ avoids the existence of the overlap region.

It is worth mentioning that $y^+ \gg y_{buf}^+$, the celebrated linear law $l_{12}^+ \approx \kappa y^+$ (where von-Karman constant $\kappa = 0.45$ from the “SED theory”), represents a “matching function” presumably between BL “inner and outer regions” with $l_0 \approx 9.7^2 \kappa/41 \approx 1.0$. The outer region can be described using the parameters r and δ , defined as the position of $0.99U_\infty$ at the BL edge with the free-stream velocity U_∞ .

However, the evaluation of δ creates a practical problem in the numerical solution to RANS equations. Specifically, two occurrences complicate any attempt in devising a proper algorithm to find the BL edge: firstly, the existence of non-uniform inviscid flow regimes, where the flow changes in the direction normal to the boundary; secondly, the appearance of spurious numerical oscillations in the flow domain. To avoid these issues, Equation (7) has been generalized for external aerodynamic applications in the current study as:

$$l_{12}^+ = l_0 \left(\frac{y^+}{9.7} \right)^{3/2} y^{+3/2} \left[1 + \left(\frac{y^+}{9.7} \right)^4 \right]^{1/8} \left[1 + \left(\frac{y^+}{41} \right)^4 \right]^{-1/4} \left[1 + \left(\frac{y^+}{130} \right)^2 \right]^{-1/2} + f_b \kappa y^+ \quad (8)$$

where f_b signifies a near-wall damping function, defined later. The modified Equation (8) identifies three layers separated at respective distances $y^+ = 9.7, 41$ and 130 , accompanied by the celebrated mixing layer. Apparently, the “SED theory” involves a set of base functions that can describe a series of successive transitions, modeling the entire profile for the whole flow domain. A multi-layer model to describe the k profile in a fully-developed BL flow can be constructed using the “SED theory” as:

$$k_a^+ = 0.131 y^{+2} \left[1 + \left(\frac{y^+}{3} \right)^2 \right]^{-1/4} \left[1 + \left(\frac{y^+}{8} \right)^4 \right]^{-7/20} \left[1 + \left(\frac{y^+}{20} \right)^6 \right]^{-1/10} \left[1 + \left(\frac{y^+}{40} \right)^4 \right]^{1/20} \quad (9)$$

Equation 9 is slightly modified from Reference (Fang & Xu, 2022) to approximate the viscous, buffer and log layers with reasonable accuracy; however, the wake-deficit layer is over-estimated, as will be seen afterward. On the other hand, “Bradshaw’s parameter” $R_b = |-uv|/k \approx \sqrt{C_\mu}$ (Bradshaw, 1967) (with the main shear-stress $|-uv|$ and $C_\mu = 0.09$) can be used to predict the k profile for wall-bounded flows. Using the SED interpolation scheme [Eq. (6)], the “stress intensity variable” R_b (parameterized with $R_T = \mu_T/\mu$) can be obtained for a fully-developed turbulent BL flow as (Rahman, 2022; and 2023):

$$R_b = \frac{C_1 R_T^{0.4}}{(1.0 + R_T)^{0.16} (1.0 + C_2 R_T^2)^{0.12}} \quad (10)$$

where $C_1 = C_\mu^{0.9}$, $C_2 = C_\mu/5.0$. As $R_T \rightarrow \infty$, $R_b \approx C_1/C_2^{0.24} \approx \sqrt{C_\mu}$. Note that R_b is extended for

wall-bounded flows from free shear flows, resolving the “near-wall turbulence”. The structure parameter R_b can be employed to calculate k profile in a BL flow as:

$$k_b = \frac{\nu_T S}{R_b + C_k} \quad (11)$$

where $\nu_T = \mu_T / \rho$ the kinematic eddy-viscosity and the near-wall singularity can be avoided with $C_k = 0.001$. Equations (9) and (11) can be interpolated to better replicate the k profile over the whole flow domain. Therefore, k and ε (dissipation-rate) profiles are evaluated as:

$$k = \frac{k_a}{3} + \frac{2k_b}{3}, \quad \varepsilon = R_b k S \quad (12)$$

Equation (12) represents an empirical hybrid modeling of the k profile. The associated function f_b in Equation (7) is modeled as:

$$f_b = R_b \tanh \left[\left(\frac{R_T}{70} \right)^2 \right] \quad (13)$$

The damping function f_b is influential in the proximity of the wall (inside the BL) and promotes the formation of the wake-deficit layer (bulk-flow structure and core layer) outside the BL.

3. NUMERICAL SIMULATIONS

The fully-developed turbulent channel flow, flat-plate BL flow and transonic flow past an RAE2822 airfoil are probably the suitable test cases to validate the performance of the ZEM. The flow equations are numerically solved using an in-house computational code, encompassing a pseudo-compressibility (PC) scheme with a “cell-centred finite-volume” formulation (Rahman and Siikonen, 2001, 2002 & 2008; Rahman 2021 and Rahman *et al.* 1997). The cell-face convective flux is evaluated using a “fully second-order” upwinding together with Roe’s damping (Rahman, 2021 and Rahman *et al.* 1997). A DDADI (“diagonally dominant alternating direction implicit”) time integration scheme has been applied to the discretized equations for the iterative solution. A multi-grid method has been employed to stabilize the solver convergence. Refs. (Rahman and Siikonen, 2001, 2002 & 2008; Rahman 2021 and Rahman *et al.* 1997) detail the salient features of coding a PC scheme. Results from the standard “shear-stress-transport” (SST) $k - \omega$ turbulence model (Menter, 1994) are convoked for comparisons.

A. Fully-Developed Turbulent Channel Flow

Fully-developed turbulent channel flows at $Re_\tau = (395; 640)$ are computed to substantiate the ZEM efficacy in replicating the near-wall turbulence. The DNS (direct numerical simulation) data are available from Refs. (Mansour *et al.*, 1988 and Kawamura *et al.*, 1999) for this

test case. A one-dimensional (1-D) RANS solver with the pressure-velocity correction method (Rahman *et al.*, 1996 & 1997 and Rahman, 2020) has been used to conduct the simulations in a channel half-width. The chosen mesh resolutions 1×64 and 1×128 grids are respectively for $Re_\tau = 395$ and $Re_\tau = 640$. Both grid arrangements are presumed to be perfect enough to reproduce the characteristic flows. The first neighbouring cell centre is at $y^+ \approx 0.3$ to ensure the viscous sublayer resolution.

Figure 1 and 2 show the computations in wall units from the ZEM and SST models. Results are plotted as: $u^+ = u/u_\tau$, $uv^+ = uv/u_\tau^2$, $k^+ = k/u_\tau^2$ and $\varepsilon^+ = \nu\varepsilon/u_\tau^4$ against y^+ . The “Boussinesq approximation” has been used to calculate the Reynolds shear stress (\overline{uv}). Remarkably, reasonable predictions of mean velocity profiles in Figs. 1(a) and 2(a) are obtained when compared with DNS data, although the ZEM neglects the transport and diffusion effects of k and ε . In contrast, the SST model under-predicts the mean velocity profiles in the wake-deficit region of BL at $Re_\tau = 640$. This deficiency perhaps arises owing to its improper choice of closure coefficients. Figures 1(b) and 2(b) represent the Reynolds shear stress profiles; both the ZEM and SST turbulence model fairly match DNS data, as can be observed.

Figure 1(c) and 2(c) execute a further assessment of the model performance with the k^+ profiles. Indicative plots of k_a^+ and k_b^+ from Equations (9) and (11) are also displayed, which have good correspondence with DNS data in the viscous sublayer and log-layer regions. As can be noticed, the ZEM fairly agrees with DNS data, whereas the SST model badly underestimates the k^+ profile in the near-wall region. Figure 1(d) and 2(d) compare the ε^+ - profiles from both turbulence models with DNS data. Note-worthily, both models are incapable of capturing the maximum magnitudes of ε^+ at the wall, approved by DNS and experimental data. However, they predict the ε^+ profiles qualitatively well after the wall region. In fact, such a behaviour of the ε^+ -profile is admitted by the SST in near-wall regimes to enhance the convergence-acceleration of the numerical solver.

B. Zero pressure-gradient flat-plate BL flow

The ZEM performance is further contrasted with the measured data of the flat-plate BL flow with a free-stream turbulence intensity $Tu_\infty = 6.0\%$ (referred to as the T3B BL case) and a reference velocity of $U_\infty = 9.4\text{m/s}$. The free-stream turbulence intensity can be given by

$$Tu_\infty = \sqrt{\frac{2}{3}} k_\infty / U_\infty$$

Experimental data are extracted from “ERCOFTAC (European Research Community on Flow Turbulence and Combustion)” Fluid Dynamics Database

(Savill, 1993). The free-stream eddy viscosity ratio $R_{T\infty} = 1.0$ is used in the current simulation. A typical non-uniform computation mesh 96×64 with a length of 1.6 m and a height of 0.3 m is shown in Figure 3. The wall-adjacent cell height is at $y^+ < 1.0$, whereas at the leading-

edge point $y^+ = 2.1$. The near-wall regions retain a heavily clustered grid. The selected grid resolution is found to be convenient in assuring a grid-independent solution (Rahman, 2022). Simulations have been prosecuted with 16 cm prior to the leading edge of the flat plate, wherein a symmetric boundary condition has been endorsed.

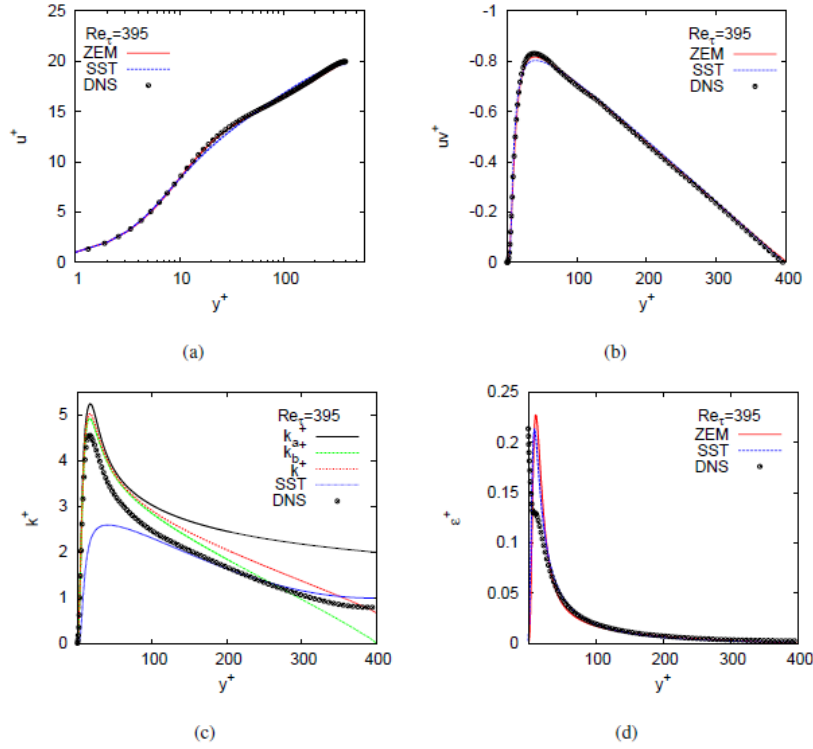


Figure 1: Mean profiles of turbulent channel flow at $Re_\tau = 395$: (a) velocity; (b) Reynolds shear stress; (c) k ; and (d) ϵ

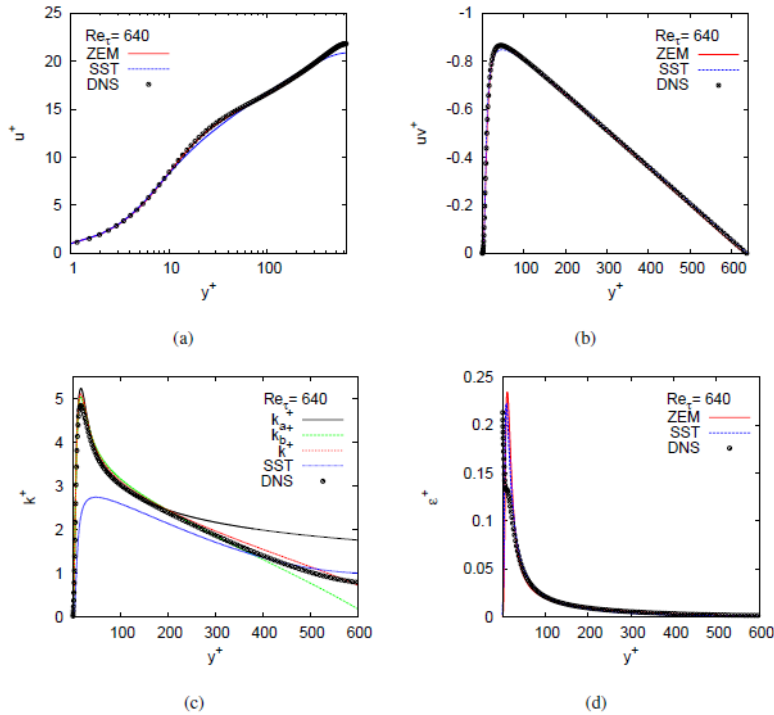


Figure 2: Mean profiles of turbulent channel flow $Re_\tau = 640$: (a) velocity; (b) Reynolds shear stress; (c) k ; and (d) ϵ

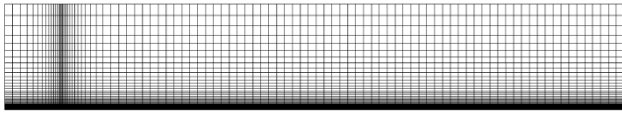


Figure 3: Representative mesh for flat-plate BL flow

Figure 4 shows the skin friction profiles ($C_f = 2u_\tau^2/U_\infty^2$) for the ZEM and SST turbulence models. As is evident, both models provide fully turbulence solutions to the T3B

BL case. The “dive” at the measured C_f distribution remains unpredicted since the selected turbulence models are insensitive to transition physics. The ZEM outperforms the SST in reproducing the experimental C_f profile along the fully turbulent regime.

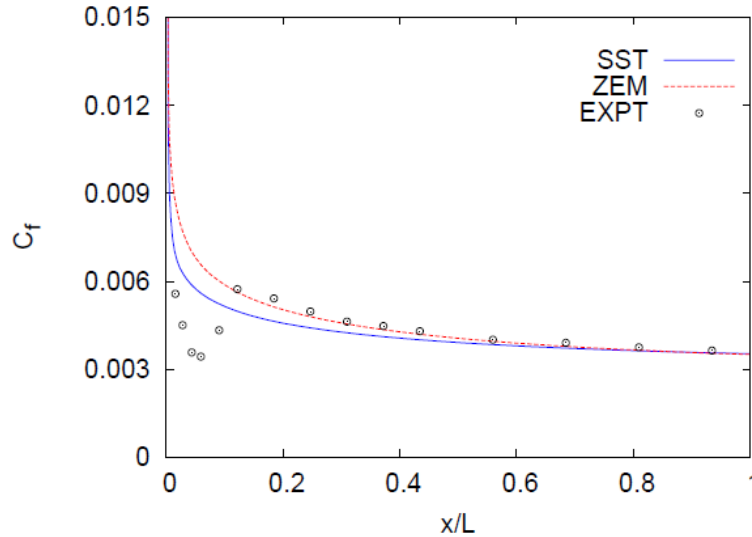


Figure 4: Skin-friction profiles for flat-plate BL case

Figure 5 represents a comparison of model predictions against measured velocity profiles of the fully-turbulent regimes at three representative positions: $x = (0.395, 0.895, 1.495)$ m. The mean velocity profiles at both BL and weak regions are well-reproduced by the ZEM when compared with experimental data. Apparently, the differences among velocity profiles in the outer layer can be explained by the predictive nature of both the ZEM and SST turbulence model in replicating C_f in Figure 4. The Reynolds shear stress and turbulent kinetic energy are plotted together with experimental data in respective Figure 6 and 7 at the same

locations. The measured total kinetic energy of turbulence is calculated using the “usual approximation $k \approx 3/4(\overline{u'u'} + \overline{v'v'})$ ” as the $\overline{w'w'}$ component is unavailable in the experiment. Conspicuously, the Reynolds shear stress profiles from both models reasonably agree with the measured data. Compared to the ZEM, the SST model underestimates the k profile in the near-wall region. The overall achievement in evaluating the friction-coefficient mean velocity and turbulence profiles is the best for the ZEM, showing an interesting feature that the ZEM agreeably mimics the measured k profile.

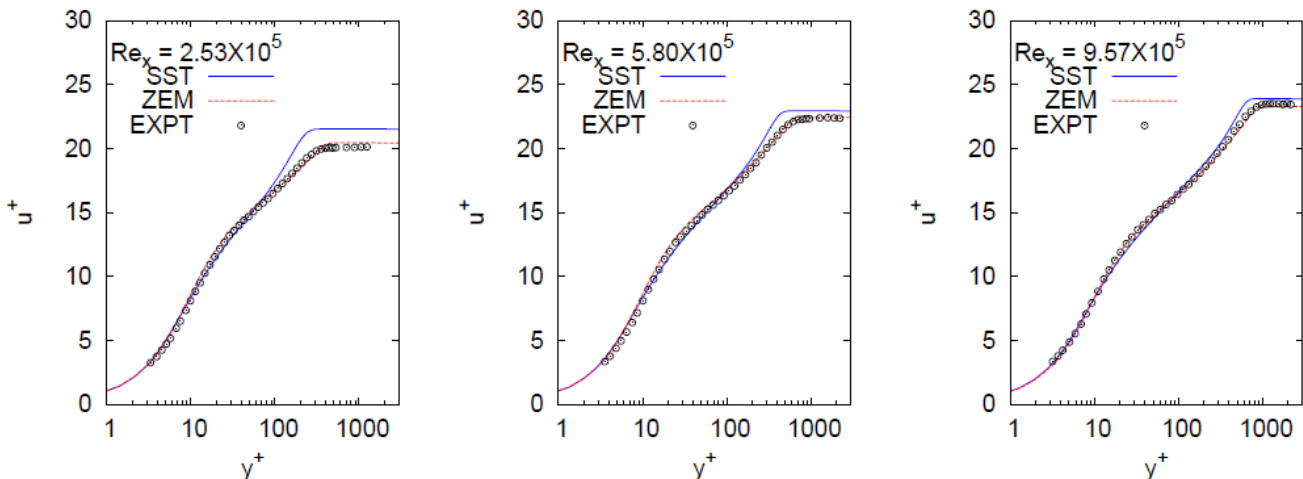


Figure 5: Mean velocity profiles for flat-plate at various downstream locations

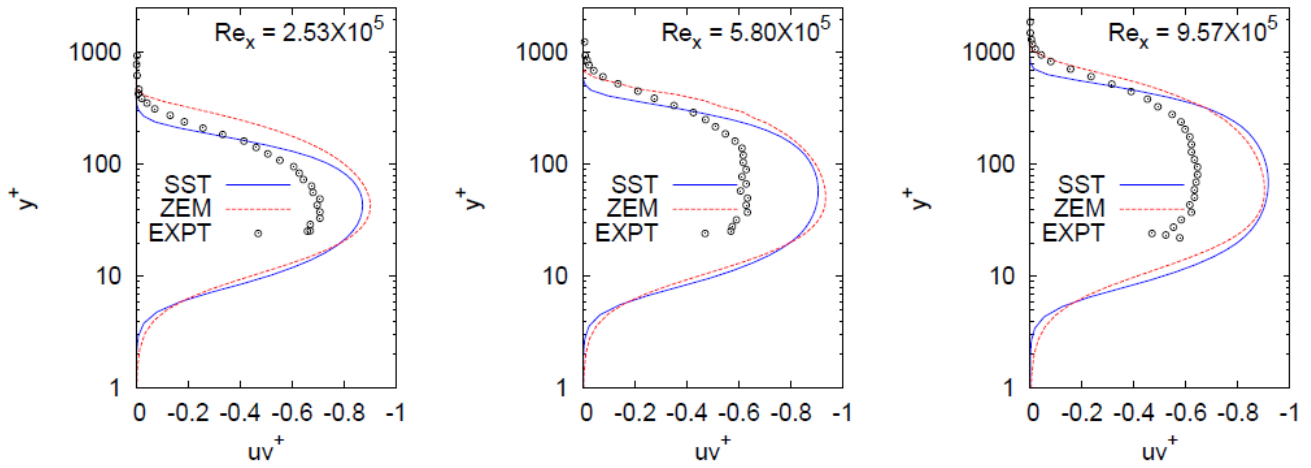


Figure 6: Reynolds shear stress profiles for flat-plate at various downstream locations

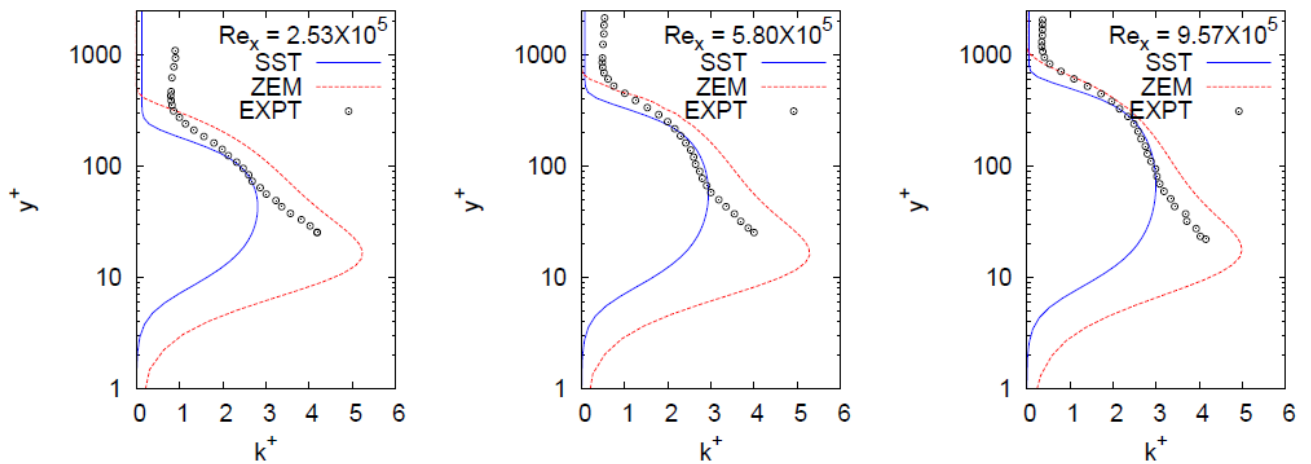


Figure 7: Kinetic energy of turbulence profiles for flat-plate at various downstream stations

C. Transonic Flow Past an RAE2822 Airfoil

The transonic flow passed an RAE2822 airfoil with strong shock-wave BL interactions is computed to justify the ZEM performance. This is a well-documented test-case for validating a new turbulence model (Cook et al., 1997; Lien et al., 1998 and Singh, 2001) with the free-stream Mach number $Ma_\infty = 0.73$, Reynolds number $Re_\infty = 6.5 \times 10^6$ and angle of attack $AOA = 2.8$ deg. Transition on both upper and lower surfaces of the airfoil in the experiment has been tripped near the leading edge at $x/c = 0.03$, where c is the airfoil cord length. The numerical methods and turbulence models influence the shock position and amount of separation (Singh, 2001). To simulate the RAE2822 airfoil, a nonuniform C-type structured grid 384×128 has been generated; 256 grid cells are allocated on the airfoil surface, which provide the wall-adjacent cell-centre at $y^+ \leq 1.0$. To better reproduce the leading-edge curvature, grid points are carefully arranged therein. Figure 8 shows the computational mesh with zoomed and full views. Far-field boundary conditions are prescribed at $40c$ away from the airfoil surface where viscous wall-boundary conditions are applied. At free-

stream boundaries, $Tu_\infty = 0.1\%$ and $R_{T_\infty} = 1.0$ are set. Computations are performed such as to match the experimental lift C_L and drag C_D coefficients, a criterion to judge the convergence.

A grid dependency study is conducted with two different grid resolutions, as shown in Figure 9. Except along the shock position indicated by the vertical lines on C_p and C_f curves, results appear to be almost grid-convergent on two-mesh levels. Therefore, a grid-independent numerical solution has been presumably ensured by the fine 384×128 non-uniform grid resolution. Figure 10 demonstrates C_p and C_f coefficients together with measured data (Lien et al., 1998; and Singh, 2001). It is clear from Figure 10(a) that the “roof-top pressure” is fairly reproduced, the shock location is predicted slightly upstream of the experimental location by the SST model and the “post-shock pressure recovery” is agreeably captured. The C_p profiles on the pressure side (lower surface of the airfoil) give similar impressions to the measured data. Figure 10(b) indicates

that C_f profiles from both models have decent match with measured data and capture the sudden change in C_f at the shock location. The ZEM detects a tiny shock-induced separation zone; however, the SST model has missed this aspect. Perhaps, the shock is too weak for the SST model with this test case to induce separation, although it is expected that the shock-induced separation may occur due to the existence of the adverse pressure gradient. Apparently, the SST turbulence model inaccurately predicts the eddy-viscosity at the shock location, causing to miss the separation. However, the ZEM captures the “essence of wall

turbulence”, signifying that the stress length (with the universal multi-layer formulation) defines the invariant wall normal distribution of the eddy-viscosity, facilitating to replicate the shock-induced separation. Due to the availability of only one measured data point on the pressure side (bottom surface) of the airfoil, no detailed comment can be made regarding the C_f coefficients. Table

1 reports the predicted C_L and C_D values from both models with measured data [26]. Qualitatively, the computed values of lift and drag coefficients from both models match the measurements.

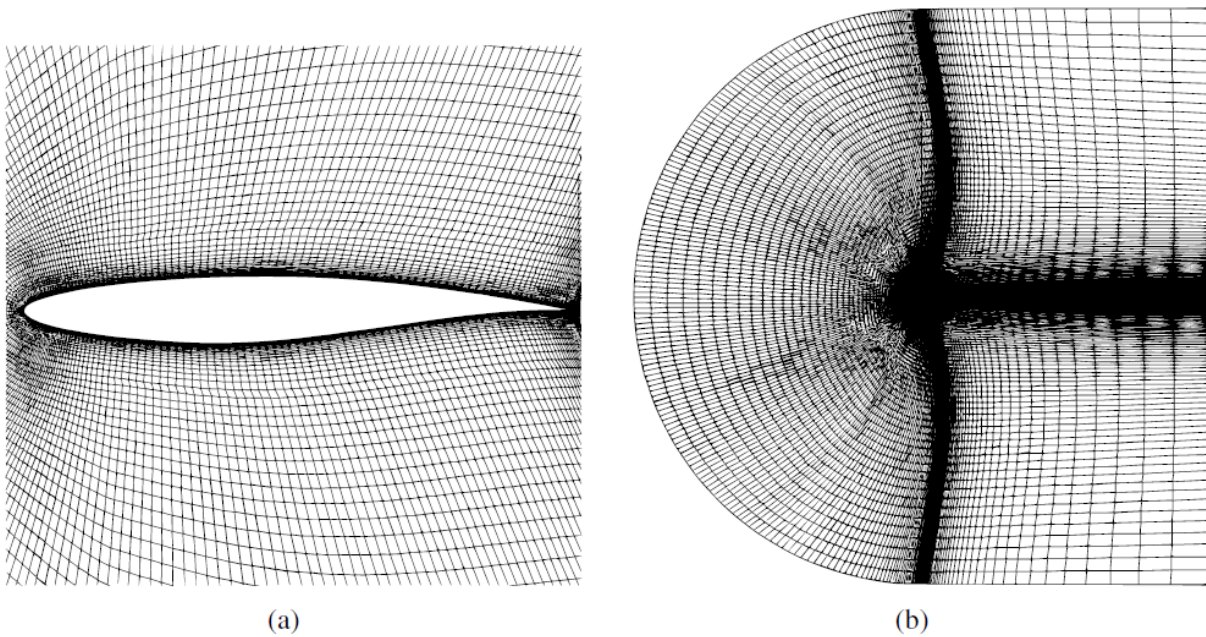


Figure 8: Computational grid for RAE2822 airfoil: (a) near-field view; (b) full view

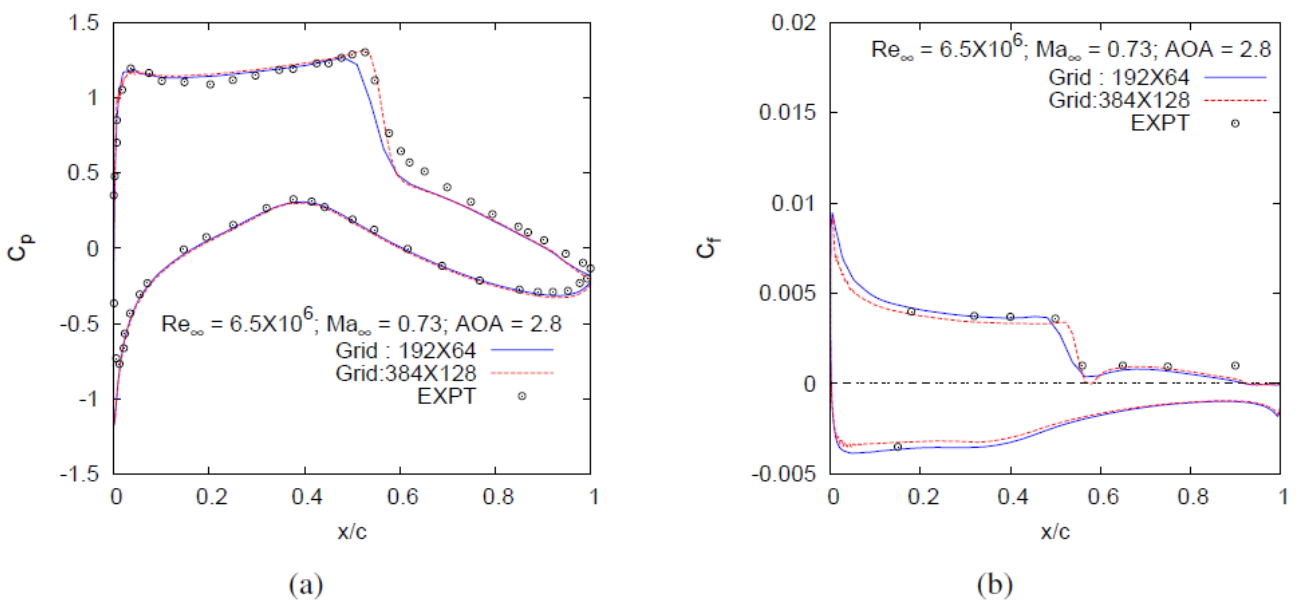


Figure 9: Effect of grid density on RAE2822 airfoil: (a) pressure coefficient profiles; (b) skin friction profiles.

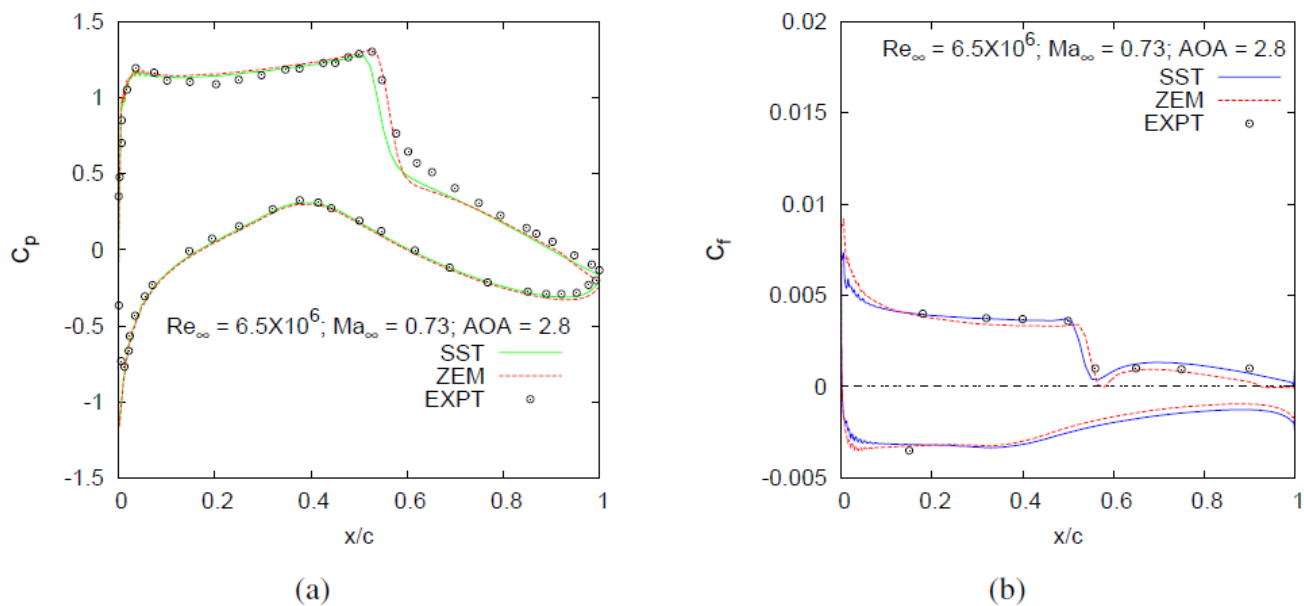


Figure 10: RAE2822 airfoil: (a) pressure coefficient profiles; (b) skin-friction profiles

Table 1
RAE2822 airfoil: lift C_L and drag C_D coefficients

AOA	Parameters	EXPT	SST	ZEM
2.8 deg	C_L	0.803	0.788	0.819
—	C_D	0.0168	0.0157	0.0165

4. CONCLUSIONS

Turbulent channel and flat-plate BL flows are computed to substantiate the ZEM efficacy in reproducing the near-wall turbulence. The RAE2822 airfoil is simulated to justify the model ability in capturing anisotropic flows with shock-wave BL interactions. Results advocate that the ZEM is competitive with the widely-used SST model. A general multi-layer representation of the stress length l_{12}^+ , adhering to the physics of wall turbulence defines the wall-normal invariant of V_T ; this aspect facilitates the success of the ZEM. The multi-layer ZEM provides an optimistic view of the RANS turbulence modelling to enhance prediction accuracies by the essence of wall turbulence. Specifically, the ZEM may induce plausible constraints on unsteady RANS, large-eddy and detached-eddy simulations. Remarkably, the multi-layer parameters such as l_0^+ and y_{bif}^+ identify the relevant flow physics of turbulent BL and the ZEM can be used to modify them for turbulence and transition modelling with the availability of experimental data.

ACKNOWLEDGMENTS

This work is financially supported by Hangzhou Dianzi University research supporting fund (Grant No.

GK218803299037 & GK228801299026) of Zhejiang Province, P.R. China.

REFERENCES

Bradshaw, P., Ferriss, D. H., & Atwell, N. P. (1967). Calculation of boundary-layer development using the turbulent energy equation. *Journal of Fluid Mechanics*, 28(3), 593-616.

Cook, P. H., Firmin, M. C. P., & McDonald, M. A. (1977). Aerofoil RAE 2822: pressure distributions, and boundary layer and wake measurements. RAE, Report AR-138, AGARD, Paris.

Fang, C., & Xu, J. (2022). Extension of the KDO turbulence/transition model to account for roughness. *Advances in Aerodynamics*, 4(1), 2. <https://doi.org/10.1186/s42774-021-00092-9>

Kawamura, H., Abe, H., & Matsuo, Y. (1999). DNS of turbulent heat transfer in channel flow with respect to Reynolds and Prandtl number effects. *International Journal of Heat and Fluid Flow*, 20(3), 196-207. doi:10.1016/S0142-727X(99)00014-4.

Lien, F. S., Kalitzin, G., & Durbin, P. A. (1998). RANS modeling for compressible and transitional flows. In *Proceedings of the summer program (Vol. 1, p. 1998)*. Stanford University USA.

Mansour, N. N., Kim, J., & Moin, P. (1988). Reynolds-stress and dissipation-rate budgets in a turbulent channel flow. *Journal of Fluid Mechanics*, 194, 15-44.

Menter, F. R. (1994). Two-equation eddy-viscosity turbulence models for engineering applications. *AIAA journal*, 32(8), 1598-1605.

Prandtl, L. (1925). Bericht über Untersuchungen zur ausgebildeten Turbulenz. *ZAMM - Journal of Applied Mathematics and Mechanics/Zeitschrift für Angewandte Mathematik und Mechanik*, 5(2), 136-139.

Rahman, M. M., Hasan, K., Liu, W., & Li, X. (2021). Predicting Fully-developed Channel Flow with Zero-equation Model. *MIST International Journal of Science and Technology*

- (MIJST), 9:17-22; 2021.
[https://doi.org/10.47981/j.mijst.09\(02\)2021.315\(17-22\)](https://doi.org/10.47981/j.mijst.09(02)2021.315(17-22))
- Rahman, M. M. (2023). Capturing transition and non-transition flows with a new shear stress transport model. *Chinese Journal of Aeronautics*, 36(3), 121-136.
<https://doi.org/10.1016/j.cja.2022.08.013>
- Rahman, M. M. (2023). Predicting transition with wall-distance-free SST $k-\omega$ model. *Computers & Fluids*, 250, 105704.
<https://doi.org/10.1016/j.compfluid.2022.105704>
- Rahman, M. M., Siikonen, T., (2001). An artificial compressibility method for incompressible flows. *Numerical Heat Transfer, Part B: Fundamentals*, 40(5), 391-409.
- Rahman, M. M., & Siikonen, T. (2002). A dual-dissipation scheme for pressure-velocity coupling. *Numerical Heat Transfer: Part B: Fundamentals*, 42(3), 231-242.
- Rahman, M. M., & Siikonen, T. (2008). An artificial compressibility method for viscous incompressible and low Mach number flows. *International Journal for Numerical Methods in Engineering*, 75(11), 1320-1340.
- Rahman, M. M. (2021). Compromising with corrector step of SIMPLE algorithm. *Mathematics and Computers in Simulation*, 188, 135-163.
- Rahman, M. M., Rautaheimo, P., & Siikonen, T. (1997). Numerical Study of Turbulent Heat Transfer from a Confined Impinging Jet Using a Pseudo-compressibility Method. In *2nd International Symposium on Turbulent Heat and Mass Transfer*, Delft, June 9-12, 1997 (pp. 511-520).
- Rahman, M. M., Miettinen, A., & Siikonen, T. (1996). Modified SIMPLE formulation on a collocated grid with an assessment of the simplified QUICK scheme. *Numerical Heat Transfer*, 30(3), 291-314.
<https://doi.org/10.1080/10407799608915084>.
- Rahman, M. M., Siikonen, T., & Miettinen, A. (1997). A pressure-correction method for solving fluid flow problems on a collocated grid. *Numerical Heat Transfer*, 32(1), 63-84.
<https://doi.org/10.1080/10407799708914999>.
- Rahman, M. M. (2020). Avoiding under-relaxations in SIMPLE algorithm. *Numerical Heat Transfer, Part B: Fundamentals*, 78(5), 310-329.
<http://dx.doi.org/10.1080/10407790.2020.1787043>.
- Rahman, M. M. (2022). Predicting transition with algebraic intermittency function. *Physics of Fluids*, 34(3), 034113.
<https://doi.org/10.1063/5.0077513>
- Savill, A. M. (1993). Some recent progress in the turbulence modelling of by-pass transition. *Near-wall turbulent flows*, 829-848, Elsevier Science, New York, 829-848.
- Segalini, A., Örlü, R., & Alfredsson, P. H. (2013). Uncertainty analysis of the von Kármán constant. *Experiments in Fluids*, 54, 1-9.
- Singh, J. P. (2001). An improved Navier-Stokes flow computation of AGARD Case-10 flow over RAE2822 airfoil using Baldwin-Lomax model. *Acta mechanica*, 151(3-4), 255-263.
- She, Z. S., Chen, X., Wu, Y., & Hussain, F. (2010). New perspective in statistical modeling of wall-bounded turbulence. *Acta Mechanica Sinica*, 26(6), 847-861.
- She, Z. S., Chen, X., & Hussain, F. (2017). Quantifying wall turbulence via a symmetry approach: a Lie group theory. *Journal of Fluid Mechanics*, 827, 322-356.
- She, Z. S., Hu, N., & Wu, Y. (2009). Structural ensemble dynamics based closure model for wall-bounded turbulent flow. *Acta Mechanica Sinica*, 25(5), 731-736.
- Townsend, A. A., (1976). *The Structure of Turbulent Shear Flow*, 2nd edition. Cambridge University Press.
- Wilcox, D. C., (2006). *Turbulence Modeling for CFD*, vol. 2. La Canada, DCW industries.